# Numerical modelling of the Sloped IPS Buoy wave energy converter

# Numerical modelling of the Sloped IPS Buoy wave energy converter

*Grégory S. Payne, Jamie R.M. Taylor, Penny Parkin, Stephen H. Salter*
School of Engineering and Electronics, University of Edinburgh
Edinburgh, Scotland

ABSTRACT
The Sloped IPS Buoy is a deep-water wave-energy converter concept whose power take-off mechanism relies on water inertia for reference. The present work deals with the modelling of this device using the higher order feature of the boundary element method package WAMIT. In a first stage, numerical predictions are compared with experimental data for a configuration where the system motion is constrained to a single degree of freedom. Comparisons are then established, initially for a free-floating configuration with no power take-off system and then with damping applied by a power take-off system.

KEY WORDS: wave energy; numerical modelling; WAMIT; experimental measurements

INTRODUCTION
The Sloped IPS Buoy concept is a floating wave energy device. Its power take-off mechanism uses water inertia for reference. This makes it possible to deploy it offshore where the deep water waves are more energetic than those in shallow coastal environments.

The concept is based on a device developed in the early nineties by the Swedish company Inter Project Services (IPS) AB. Their device consisted of a vertical heaving buoy with a power take-off mechanism that carries its own internal reaction mass in the form of a body of water contained within a large vertical tube which is open to the sea. The tube, rigidly connected to the buoy, is blocked by a piston that can slide along its axis. As wave action induces vertical motion of the buoy and tube, the piston tends to stay relatively stationary due to the large added inertia of the water above and below it. There is therefore a relative motion between the piston and the buoy which can be used to drive a hydraulic ram. An important feature of this power take-off mechanism is the technique used to address the end-stop problem. It is achieved by enlarging the inner diameter of the tube at positions that correspond to the end positions of the hydraulic ram. Water is then able to flow around the piston to create a significant reduction in its hydrodynamic loads. More information on the original IPS device can be found in (Bergdahl, 1992). A schematic diagram of the device is shown in Fig. 1.

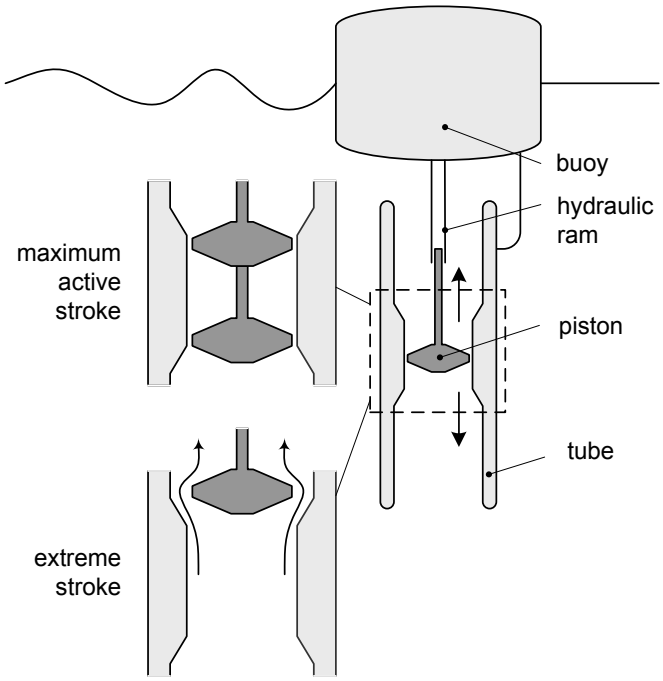


Fig. 1: Principle of the IPS power take-off mechanism. The close-up view at top left shows the two end positions of the piston in the case of a maximum active stroke. The lower close-up view shows the position eventually reached by the piston in the case of an extreme wave, with the water flowing around it.

The contribution of the University of Edinburgh to the development of the IPS concept is the idea of using slope motion to try to make the device more efficient in the more energetic longer waves. The hydrostatic stiffness force is vertical and directed upwards. The magnitude of this force when resolved along a slope direction at any angle from vertical will be some fraction of this value. By constraining the buoy motion to such a slope direction, its linear hydrostatic stiffness will therefore be lower than if it were moving vertically. This is illustrated in Fig. 2.

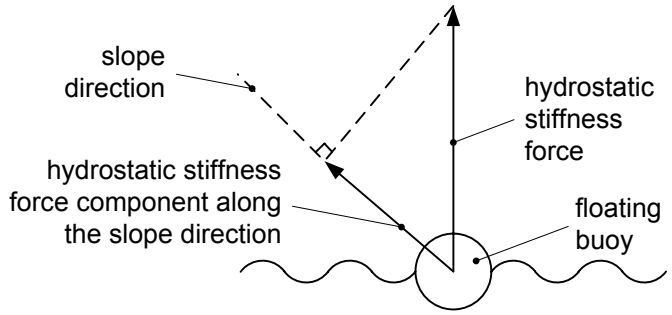


Fig. 2: For a buoy moving in a slope direction the apparent stiffness due to buoyancy is reduced.

The mass of the device remains constant, regardless of the direction of motion and so its resonant period tends to be higher when the motion is sloped than when it is vertical.

This paper deals with the numerical modelling of the Sloped IPS Buoy using the boundary element method package WAMIT. The study comprises three distinct stages.

1. In order to investigate the concept of sloped motion, a simplified one degree of freedom version of the system is considered by externally constraining the buoy motion to translation along the slope direction. The power take-off mechanism is referenced to the sea bed.
2. A free-floating version of the system is considered with the power take-off tube fitted but disabled.
3. The free-floating system is fitted with an active power take-off mechanism that applies damping to the relative motion between the piston and the tube.

For each of these stages, numerical predictions are compared with experimental results. The numerical modelling is based on a frequency domain approach and only regular waves are considered.

## NUMERICAL MODELLING

The numerical modelling is carried out using WAMIT (Wave Analysis Massachusetts Institute of Technology). It is based on the boundary element method and was developed for the analysis of wave-body interaction. Its main field of application lies in the offshore industry (Newman and Sclavounos, 1988) but it has also been used more recently to model wave energy converters (Lee, Newman *et al.*, 1996; Delauré and Lewis, 2003). The computations presented here are based on a linear theory of hydrodynamic which relies on the following assumptions.

- Incompressibility and constant density fluid
- Zero viscosity
- Irrotationality
- No surface tension
- Linearization of the free surface boundary conditions
- Linearization of the body surface boundary conditions
- Linearization of the Bernoulli's equation

The validity of such assumptions is a complex issue and is often specific to the hydrodynamic problem considered (Payne, 2006). However, there is a consensus that low steepness waves and small amplitudes of motion can usually be modelled reliably (Zienkiewicz, Lewis *et al.*, 1978).

The conventional approach of the boundary element method relies on a piecewise representation of the velocity potential over the body surface. This is achieved by discretizing the body geometry into flat panels over which the velocity potential is assumed to be constant. This approach is often referred to as the low-order method. In recent versions of WAMIT an alternative approach, called the higher order method, offers the possibility of representing both the body geometry and the velocity potential on the body by using B-Spline surfaces. These are continuous piecewise polynomial parametric surfaces which are mainly defined by sets of control points. More detail on B-Splines can be found in (Mortenson, 1997). The higher order method leads in most cases to more efficient computations (Lee, Maniar *et al.*, 1996).

The accuracy of the numerical prediction of body responses in waves is directly influenced by the accuracy of the representation of the velocity potential over the body surface. Improving the accuracy of this representation increases the computational burden, but too inaccurate a representation can lead to divergence of the solution. It is therefore important to carry out convergence tests against the most accurate solution practically obtainable. For space reasons, these convergence tests have not been included here but can be found in (Payne, 2006).

A CAD package called MultiSurf can be used to produce B-Spline body geometries. This software was primarily developed as a tool for yacht designers to help them explore and draft hull surfaces. Alternatively, body geometries can be defined analytically by coding parametric equations that represent the body surface in the form of Fortran routines.

## SINGLE DEGREE OF FREEDOM CONFIGURATION

The single degree of freedom approach to the Sloped IPS buoy was investigated experimentally by Chia-Po Lin during his PhD (Lin, 1999) as a preliminary study of the concept.

### Experimental Equipment

The experiments were carried out in the original Edinburgh wide tank using a model scaled to around 1/75$^{th}$.

#### *Experimental Model*

The single degree of freedom model, shown in Fig. 3, consisted of a semi-cylindrical float that could slide along a sloped guide-tube on a water-fed hydrostatic bearing that minimised frictional losses.

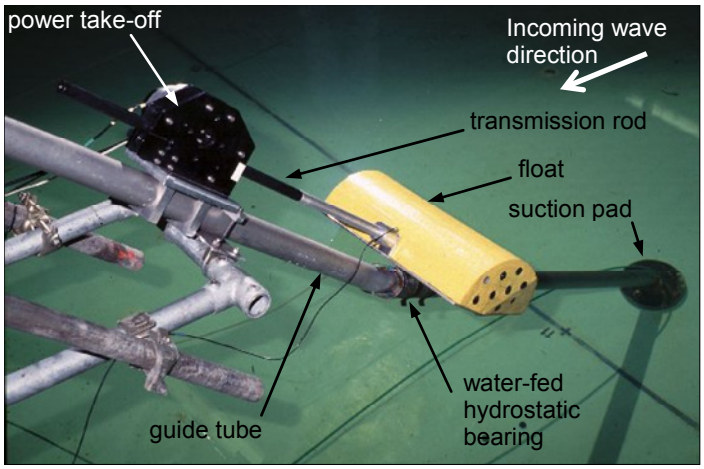


Fig. 3: The single degree of freedom model

The guide-tube could be set at different angles to the water surface by an external scaffolding arrangement on one side and by a suction pad on the other side. A transmission rod provided a mechanical connection between the float and the power take-off mechanism. It also prevented rotation of the float with respect to the guide-tube axis. The power take-off which provided a means of damping the float motion was simulated by a low inertia DC motor fitted with a tachometer that gave velocity information. This operated in conjunction with a piezo-electric force

sensor placed between the transmission rod and the float. The float was 0.5m wide and 0.3m in diameter.

Slope angle was measured with respect to the horizontal. Four values were investigated: 90° (pure heave motion), 60° 45° and 35°.

***The Wide Tank***

The experimental testing of the model took place in the Edinburgh wide tank. It was constructed in 1977 specifically for wave energy research. It was originally designed to test a crest-spanning free-floating 'duck' string (Salter, Jeffrey *et al.*, 1976) at a scale of $1/150^{th}$ in waves representative of North Atlantic sea conditions. It was dismantled in 2001.

The tank was 27.5m wide. Its useful length (between the wave-makers and the beaches) was 7.3m. The water depth was 1.2m. The waves were generated by 89 rolling-seal flap-type wave-makers at a pitch of 305mm. The control strategy for the wave-makers was based on force and velocity feedback, so that whilst generating the intended waves they could also absorb the energy of reflected and parasitic waves.

**Numerical Considerations**

The geometry input to WAMIT for the single degree of freedom configuration was defined analytically. Fig. 4 shows the wire mesh representations of the four configurations investigated. These correspond to the 90°, 60° 45° and 35° slope angles. Only the part of the float located below the mean water level need be defined. This is because the free surface and body surface boundary conditions are linearized. Consequently wave loads are computed only on the averaged wetted surface of the body (Newman, 1977).

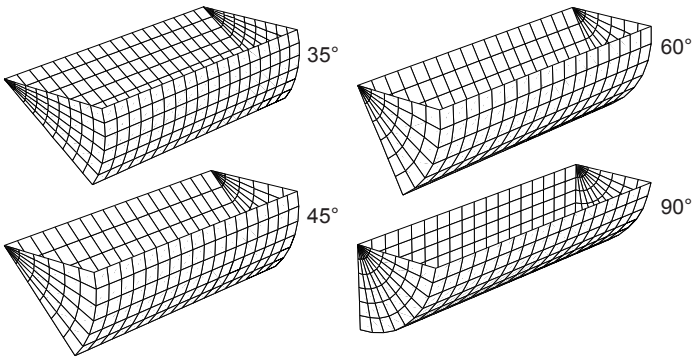


Fig. 4: Wire frame views of the geometrical input for the single degree of freedom configuration

**Power Take-Off Control Strategy**

For a single degree of freedom system in regular waves, the optimum power take-off damping can be calculated analytically. To do so, it is useful to introduce the concept of hydrodynamic impedance.

***Hydrodynamic Impedance***

From an experimental point of view, the hydrodynamic impedance is usually measured in the absence of incident waves. It is obtained by driving the model with a sinusoidal force.

The model can be considered as a simple dynamic system. The input is a harmonic force, provided by the DC motor that acts parallel to the guide-tube.

The output of the system is the model velocity along the same axis. The hydrodynamic impedance $Z(\omega)$ is the transfer function between input and output:

$$Z(\omega) = \frac{F(\omega)}{U(\omega)} \tag{1}$$

where $F(\omega)$ is the harmonic force applied to the float and $U(\omega)$ is the float velocity. Since $F(\omega)$ and $U(\omega)$ are generally not in phase, $Z(\omega)$ is complex. The real part of the hydrodynamic impedance corresponds to the radiation damping. The imaginary part is associated with the inertia of the model (including the added mass) and the hydrostatic stiffness.

***Optimum Power Take-Off Damping***

For a single degree of freedom device whose power take-off is referenced to the sea bed, it can be shown (Lin, 1999) that the average extracted power $P$ is given by:

$$P = \frac{|F_e|^2}{4(D_a + |Z|)} \cdot \left( 1 - \frac{(B - |Z|)^2}{|B + Z|^2} \right) \tag{2}$$

where $Fe$ is the wave exciting force, $D_a$ the radiation damping, $Z$ the hydrodynamic impedance as defined by Eq. (1) and $B$ the damping applied to the float motion by the power take-off.

From Eq. (2) it can be seen that $P$ is maximum for:

$$B = |Z| \tag{3}$$

**Results**

For each wave frequency investigated, the power take-off mechanism was set to provide the optimum damping given by Eq. (3). Numerical predictions and experimental measurements are compared in terms of 'capture width', the ratio of the power captured by the system to the power available in a wave front of the same width as the device. The latter was experimentally evaluated by recording the wave elevation at the place of the model but in its absence. From the recorded wave amplitude $a$, the wave power density $P_d$ in Watt per meter of wave front is computed by:

$$P = \frac{\rho g^2}{8\pi} a^2 T \tanh kh \left( 1 + \frac{2kh}{\sinh 2kh} \right) \tag{4}$$

where $\rho$ is the water density, $g$ the gravitational acceleration, $T$ the wave period, $k$ the wave number and $h$ the water depth.

Fig. 5 shows a comparison between experimental and numerical results for the four slope angles. The continuous lines correspond to the WAMIT predictions and the crosses to the experimental data. The agreement is generally good but the experimental points appear to fluctuate around the numerical line. This 'ripple noise phenomenon' is believed to be caused by waves reflecting off the tank boundary and interfering with measurements at the model location

In places the capture width exceeds 100%, which means that the system was absorbing more wave energy than was incident in the width of the device. This phenomenon is generally known by the term 'point' absorption. It was first investigated in the 1970s by (Budal and Falnes, 1975), (Newman, 1976) and (Evans, 1976).

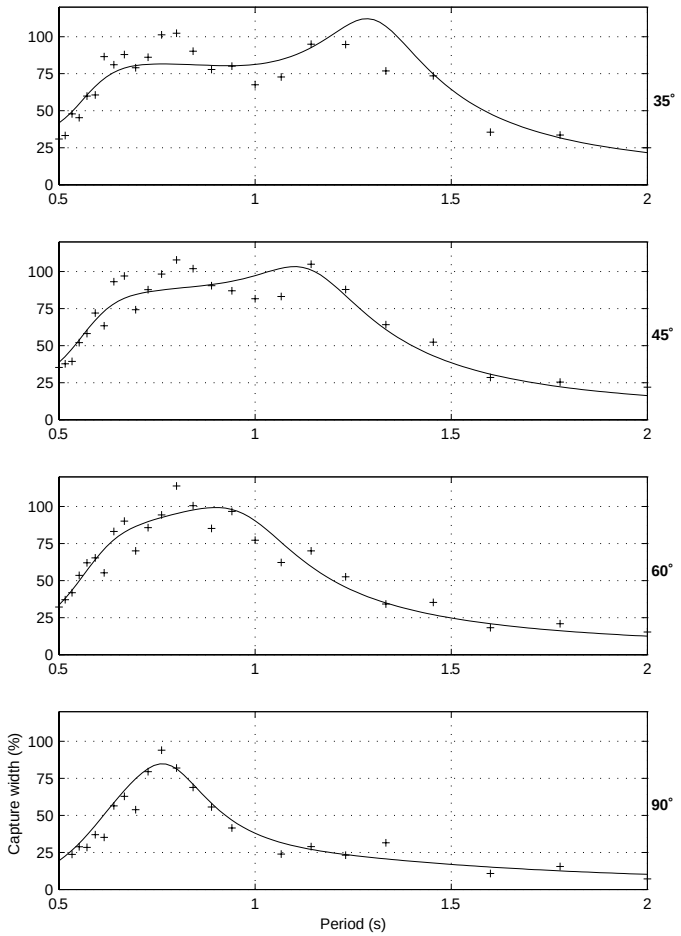


Fig. 5: Single degree of freedom configuration. Capture width in percent plotted against wave period for four slope angles. The crosses correspond to experimental measurements and the solid line to WAMIT predictions.

FREE-FLOATING CONFIGURATION WITHOUT POWER TAKE-OFF

The leap from the single degree of freedom configuration to a free-floating system whose power take-off reacts against water inertia is a large one. It was therefore thought desirable to investigate an intermediate stage, a free-floating device with no power take-off mechanism.

**Experimental Equipment**

The free-floating model was tested in the new Edinburgh 'curved' tank. Motions were recorded with a video tracking system.

***Experimental Model***

The experimental model consisted of a float, a tube and an 'inertia' plate as shown in Fig. 6.

The float was made of closed-cell (density 100kg.m$^{-3}$) polyurethane foam. This material is easy to machine, has low density and has a finer texture and greater robustness than polystyrene.

The inertia-plate was conceived of as a way to constrain the device motion to the slope direction by providing added inertia in the direction perpendicular to the plate.

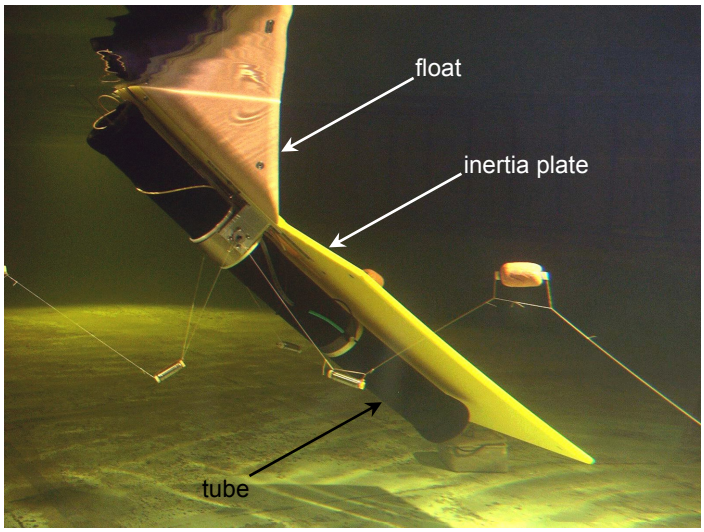


Fig. 6: Underwater view of the free-floating model. The waves are coming from the right.

The tube forms part of the power take-off mechanism. During the first set of experiments the piston was not fitted and the tube was open at both ends. Ideally, both openings of the tube would be located at a depth where the flow is largely unaffected by wave orbital motion. This was limited in the experiment by the depth of the tank and the length of the tube.

The model was moored to the bottom of the tank using three compliant float and sinker moorings as shown in Fig. 6 (two were on the incident wave side and the other to the rear).

***The Edinburgh 'Curved' Tank***

The 'curved' tank was built using wave-making paddles recovered from the wide tank. The water depth is still 1.2m. The array of 48 wave-makers is arranged as a 9 m radius arc whose included angle is just over 90° (see Fig. 7). Further details of the tank can be found in (Taylor, Rea *et al.*, 2003).

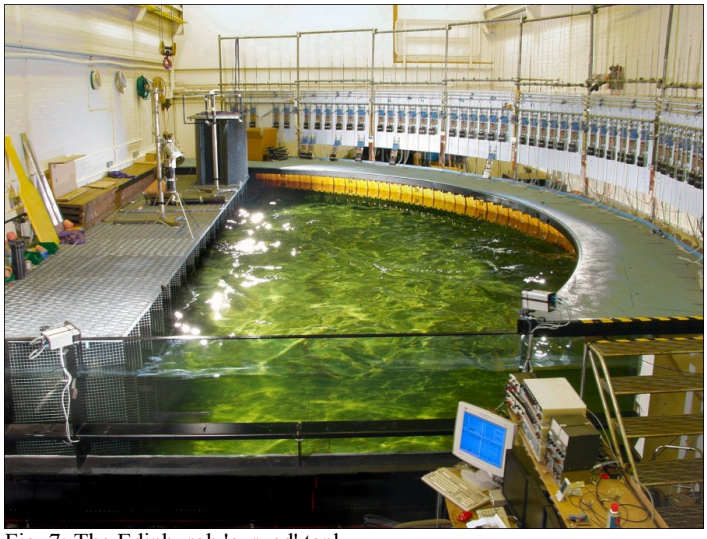

Fig. 7: The Edinburgh 'curved' tank

***The Video Motion Tracking Device***

The curved tank is fitted with a MarineTrak system manufactured by the Swedish company Qualisys Medical AB. Two of their special video

cameras are installed.
The system provides real time displacement information for the six degree of freedom of the model without interfering in any way with its motions.

The measurement technique relies on the principle of triangulation. The two infrared sensitive cameras are set to view the area where the model moves. The measurement volume is defined by the overlap of the respective camera fields of view. The cameras detect the position of small reflecting-ball markers attached to the model. Two-dimensional position data from each camera is sent to a central processing unit where it is combined with camera location information, to compute the three-dimensional co-ordinates of the markers.

With the configuration used for these experiments, the nominal linear resolution of the MarinTrak system was ±0.1mm. The sampling frequency was 32Hz.

**Input Geometry to WAMIT**
The geometrical input to WAMIT was generated using the CAD package MultiSurf. A solid view of the geometry is given in Fig. 8.

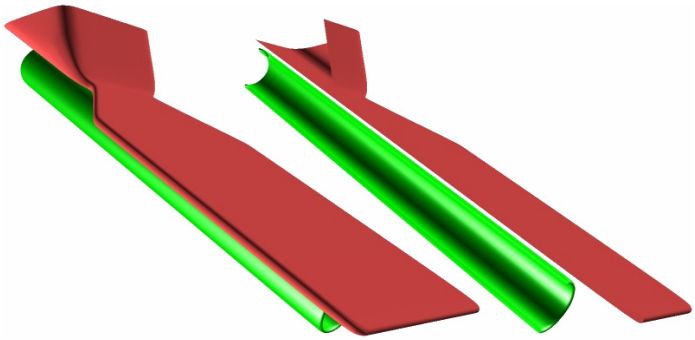

Fig. 8: Rendered views of the geometry corresponding to the free-floating model without power take-off. The section view on the right shows the representation of the tube with no piston.

**Results**
The comparison between numerical predictions and experimental results was established in terms of body response. Since the direction of propagation of the waves is parallel to the plane of symmetry of the model, only the body response in this plane is reported.

The comparison in Fig. 9 focuses on the motion of a point located at the top of the float. This motion is decomposed into horizontal (surge) and vertical (heave) components. These are normalised by the wave amplitude.

In the case of the heave motion, the agreement is generally good. However, the amplitude of the resonance peak predicted by WAMIT is considerably higher than that observed experimentally. This difference can fairly be attributed to the neglect within the numerical model of parasitic energy losses due to flow viscosity.

In the case of surge, numerical predictions and experimental data show the same underlying trend. However, the experimental measurements are strongly affected by the ripple noise that has already been referred to. This again is assumed to be due to reflections form the tank boundaries.

The ripple noise phenomenon does not visibly affect the heave measurements. The motion amplitudes shown in Fig. 9 are normalised by the measured wave amplitude. This has the effect that the normalised heave motions become fairly independent of wave reflection, whilst those in surge are strongly affected by reflections.

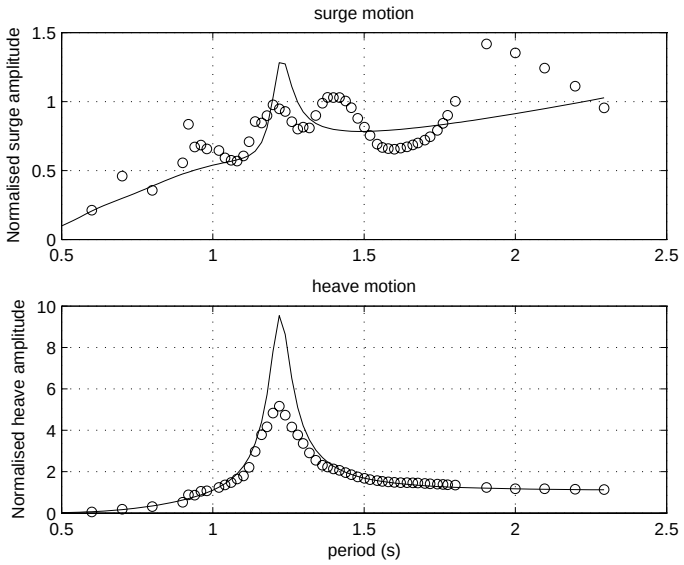


Fig. 9: Normalised surge and heave motion of the free-floating device without power take-off plotted against wave period. The solid lines correspond to the WAMIT predictions and the circles to experimental data.

To understand this, it is useful to consider the simplified case where the floating model is small with respect to the wavelength and is located in a deep water unbounded wave field. The heave motion will follow the free surface, and so the normalised heave response will be unity. From the small body approximation, the surge response will follow the horizontal motion of the water particles. As these have a circular motion in deep water waves, the normalised surge response will also be unity. Now consider the case of a fully reflective wall behind the model. This will generate a standing wave pattern and the heave response of the model will now depend on its location. If at an anti-node it will be doubled. However, the normalising process will again yield a normalised heave response of unity, since at the anti-node, the wave amplitude has doubled. This argument holds true for any location of the model, so the normalised heave response of the small model is not affected by its location on the standing wave pattern.

In contrast, the location of the model does affect the normalising of the surge response. If at an anti-node, the model will not have any surge motion. If at a node, the surge response will be twice what it would be without reflection. In the vicinity of an anti-node, the next to zero surge motion amplitude is divided by nearly twice the regular wave amplitude. Near a node, the doubled surge amplitude is divided by a wave amplitude close to zero. In shallow water the discrepancy is increased. In conclusion, in the real world of a test tank, normalised heave responses tend to be relatively unaffected by ripple noise, whilst surge responses tend to be strongly affected.

FREE-FLOATING CONFIGURATION WITH POWER TAKE-OFF
The free-floating experimental model is again as shown in Fig. 6.

**The Dynamometer**
The dynamometer used with the model relies on the ‘eddy-current damper’ phenomenon. Fig. 10 shows a cut-away section.

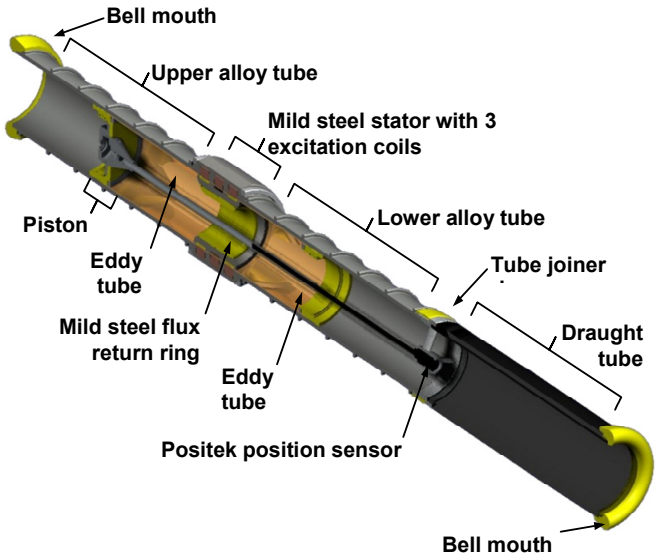


Fig. 10: Sectional view of the dynamometer

The excitation coils create a magnetic field which circulates through the mild steel stator and flux return ring. In the gap between those two parts, the field is orientated radially. The eddy-tube slides axially through this 1.5mm wide gap. This motion, perpendicular to the magnetic field, induces a circumferential voltage in the tube, which in turns drives a current through its resistance. This current, in combination with the radial magnetic field, now generates a force which tends to oppose the motion of the eddy tube. The force is proportional to the axial velocity of the eddy tube, and provides very 'clean' damping forces. The damping coefficient is proportional to the square of the coil current.

The piston is fitted with a 'Positek' linear displacement transducer measuring the position of the tube with respect to the surrounding tube.

In order to locate the eddy tube axially and to enable it to slide without contact against the outer tube, hydrostatic water fed bearings are fitted to both ends of the eddy-tube and to the mild steel flux returning ring. Further detail on the dynamometer can be found in (Taylor and Mackay, 2001).

**Modelling of the Power Take-Off**

The power take-off mechanism is not referenced to the seabed and energy is captured from the relative motion between the piston and the surrounding tube. From a modelling point of view, this means that the overall system cannot be modelled as a single rigid body. Instead, the device is treated as two separate sub-systems, one being the piston and the other comprising the tube, the plate and the float. Special attention is required in the model definition to ensure that the motion of the two bodies is properly coupled, to avoid 'non-physical' motions such as the piston moving radially through the tube. More detail on the modelling of the power take-off mechanism can be found in (Payne, 2005). The input geometry is shown in Fig. 11.

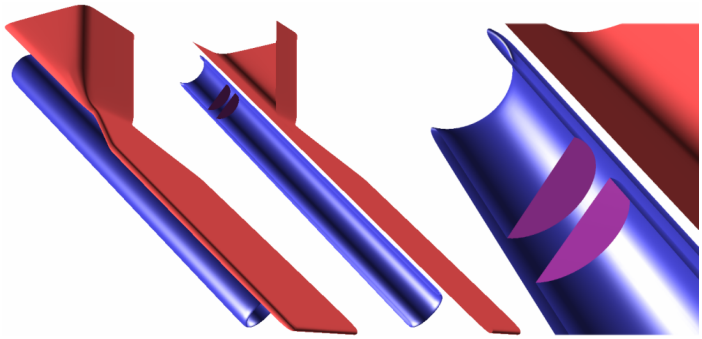

Fig. 11: Rendered view (left) of the geometry corresponding to the free-floating model without power take-off. The section views (middle and right) shows the representation of the tube and of the piston.

**Results**

Two damping values were investigated: 3.45 and 14.17 kg.s$^{-1}$. Numerical predictions and experimental data are compared in terms of body response and piston motion. The body response is measured in a similar way to that used for the free-floating model without power take-off. Piston motion is treated as the relative motion between it and the tube. Fig. 12 shows results for body motions normalised by wave amplitude.

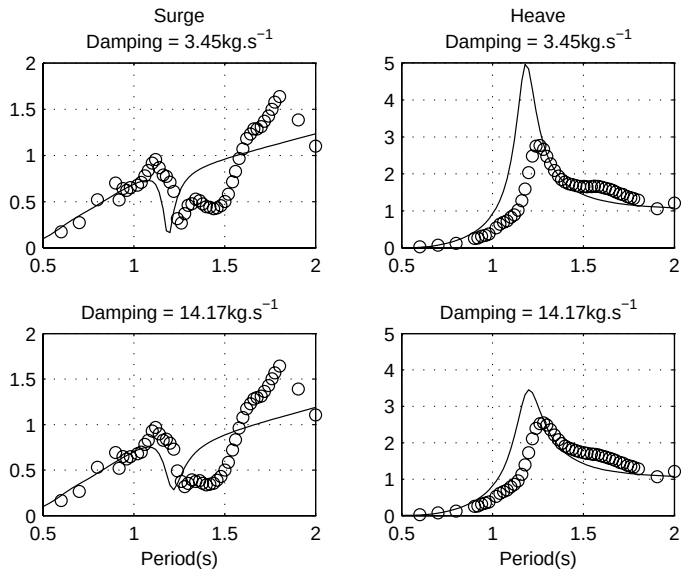


Fig. 12: Surge (left) and heave (right) components of the normalised motion of the free-floating configuration with power take-off for two damping values. Solid lines correspond to WAMIT predictions and circles to experimental measurements.

In the surge results, numerical predictions and experimental data exhibit similar trends. However, as for the free-floating configuration without power take-off, the experimental measurements are affected by ripple noise. Experimental points and numerical curves plunge sharply for wave periods in the vicinity of 1.2 s. There is however a small relative offset of about 0.06 s in the wave period for which this plunge takes place.

In the heave results the shapes of the experimental and numerical curves are broadly similar. In each case, a peak occurs at the same wave period as the drop-off in surge response. As in surge, there is a difference of about 0.06 s in the wave period for which this peak occurs between experimental and numerical values. The amplitude of the peak of the numerical prediction is about 65% higher than the experimental one for

the low damping case. This discrepancy in amplitude reduces with higher damping. A possible interpretation for this phenomenon is that WAMIT does not take into account viscous damping. This can lead to predictions of very large responses at resonance and is probably the case for the low damping setting. However, as the dynamometer damping is increased, the viscous damping could become less significant with respect to the dynamometer damping. In other words, the overall damping in the physical experiment would be largely dominated by the dynamometer damping. This would yield a better amplitude match with numerical predictions since the dynamometer damping is taken into account in the numerical model.

Piston motions normalised by wave amplitude are shown in Fig. 13.

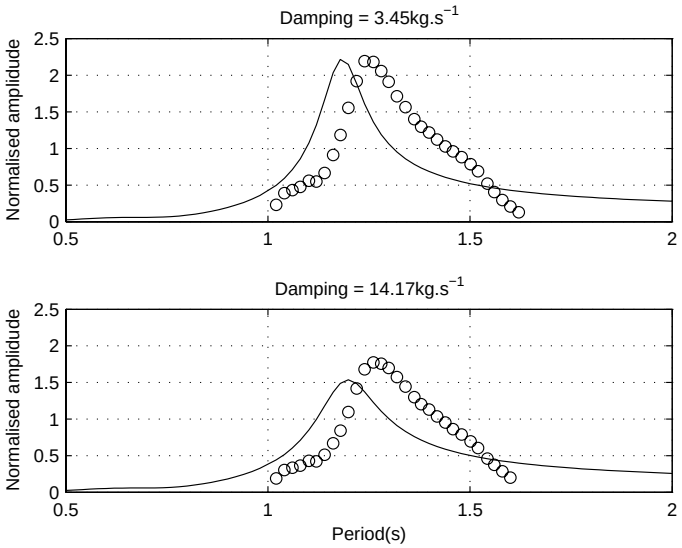


Fig. 13: Motion of the piston relative to the surrounding tube for two power take-off damping values. The circles correspond to the experimental measurements and the solid lines to WAMIT predictions.

The general trend of both experimental measurements and the numerical data is similar, in that they both exhibit a peak. The frequency of this peak corresponds to the peak in heave response and to the sharp plunge in surge response (Fig. 12). As for the surge and heave responses, there is a shift of about 0.06 s between numerical and experimental responses for the period at which the peak occurs.

## CONCLUSION

Three configurations of the Sloped IPS Buoy were modelled using the boundary element method package WAMIT. The outcome of these models has been compared with corresponding experimental measurements.

For the single degree of freedom configuration, the agreement is good.

For the free-floating configuration without power take-off, the WAMIT model reasonably predicts the response trend observed experimentally but overestimates the response amplitude at resonance.

For the free-floating configuration with power take-off numerical predictions exhibit the same trend as experimental measurements but with a discrepancy of 0.06s in the wave period for which resonance takes place.

For the three configurations, experimental data are affected by wave reflection from the tank boundaries. This phenomenon is not taken into account in the numerical model where the fluid domain is considered infinite.

The boundary element method does not take into account parasitic losses due to flow viscosity. This leads to overestimation of the device heave response. For the free floating configuration the magnitude of the overestimation varies with and without the power take-off mechanism.


## ACKNOWLEDGEMENT

This work has been supported by two UK agencies: the Engineering and Physical Sciences Research Council, partly through the SuperGen-Marine Research Consortium and the Department of Trade and Industry.


## REFERENCES


Bergdahl, L. (1992). "Review of research in Sweden". *Wave energy R&D workshop*, Cork, Ireland, pp. 129-136.

Budal, K. and Falnes, J. (1975). "A resonant point absorber of ocean-wave power", *Nature*, vol. 256, pp. 478-479.

Delauré, Y. M. C. and Lewis, A. (2003). "3D hydrodynamic modelling of fixed oscillating water column wave power plant by a boundary element methods", *Ocean Engineering*, pp. 309-330.

Evans, D. V. (1976). "A theory for wave-power absorption by oscillating bodies", *Journal of Fluid Mechanics*, vol. 77, part 1, pp. 1-25.

Lee, C.-H., Maniar, H., Newman, J. N. and Zhu, X. (1996). "Computations of Wave Loads Using a B-Spline Panel Method". *21st Symposium on naval hydrodynamics*, Trondheim, Norway, pp. 75-92.

Lee, C.-H., Newman, J. N. and Nielsen, F. G. (1996). "Wave Interactions with an Oscillating Water Column". *6th International Offshore and Polar Engineering Conference*, Los Angeles, USA, vol. 1, pp. 82-90.

Lin, C. P. (1999). *Experimental studies of the hydrodynamic characteristics of a sloped wave energy device*. PhD thesis, University of Edinburgh, Scotland.

Mortenson, M. E. (1997). *Geometric Modeling*, John Wiley & Sons.

Newman, J. N. (1976). "The interaction of stationary vessels with regular waves". *11th Symposium on Naval Hydrodynamics*, London, pp. 491-501.

Newman, J. N. (1977). *Marine Hydrodynamics*, The MIT Press.

Newman, J. N. and Sclavounos, P. D. (1988). "The computation of wave loads on large offshore structures". *Conference on the Behaviour of Offshore Structures (BOSS `88)*, Trondheim, Norway, vol. 2, pp. 605-622.

Payne, G. (2005). "Hydrodynamic modelling of a generic power take-off mechanism reacting against water inertia". *Sixth European Wave and Tidal Energy Conference*, Glasgow, Scotland, to be published

Payne, G. (2006). *Numerical modelling of a sloped wave energy device*. PhD thesis, University of Edinburgh, Scotland.

Salter, S. H., Jeffrey, D. C. and Taylor, J. R. M. (1976). "The architecture of nodding duck wave generators", *The Naval Architect*, pp. 21-24.

Taylor, J. R. M. and Mackay, I. (2001). "The design of an eddy current dynamometer for a free-floating sloped IPS buoy". *Marine Renewable Energy Conference (MAREC)*, Newcastle upon Tyne, UK, pp. 67-74.

Taylor, J. R. M., Rea, M. and Rogers, D. J. (2003). "The Edinburgh curved tank". *Fifth European Wave Energy Conference*, Cork, Ireland, pp. 307-314.

Zienkiewicz, O. C., Lewis, R. W. and Stagg, K. G. (1978). *Numerical Methods in Offshore Engineering*, John Wiley & Sons.